Catalysis Today 179 (2012) 16–26

Contents lists available at ScienceDirect

Catalysis Today

journal homepage: www.elsevier.com/locate/cattod

Study of the structure directing effect of the chiral cation (1S,2S)-2-hydroxymethyl-1-benzyl-1-methylpyrrolidinium in aluminosilicate preparations in the presence of co-structure directing agents

Raquel García*, Luis Gómez-Hortigüela, Joaquín Pérez-Pariente

Instituto de Catálisis y Petroleoquímica (CSIC), C/Marie Curie 2, 28049 Cantoblanco, Madrid, Spain

ARTICLE INFO

Article history:
Received 9 May 2011
Received in revised form 1 July 2011
Accepted 11 July 2011
Available online 3 September 2011

Keywords:
Zeolite synthesis
Co-structure directing agents
MWW zeolite family
Molecular modeling

ABSTRACT

We explore the structure directing role of the chiral cation (1S,2S)-2-hydroxymethyl-1-benzyl-1-methylpyrrolidinium (SS-bmpm) in the synthesis of Al-containing zeolite materials in the presence of co-structure directing agents (co-SDAs). Three different co-SDAs are studied: tetramethylammonium (TMA), quinuclidine and sodium. Synthesis with TMA as co-SDA yields a ferrierite related phase and a material from the MWW family, where the SS-bmpm and the TMA cations are incorporated intact within the samples. Quinuclidine produces instead amorphous solids, while the use of Na^+ leads to crystalline phases that crystallized as a result of the degradation of the SS-bmpm cation. A subsequent computational study based on molecular mechanics was performed in an attempt to unravel the location of TMA and SS-bmpm cations within the void space of the complex MWW structure. The results suggest that the sinusoidal channels are exclusively filled by TMA, while the bulky SS-bmpm cations can only be accommodated within the MWW super-cages, thus providing a new example of cooperative structure-directing effects of small and bulky cations in the synthesis of complex zeolite structures.

1. Introduction

Zeolites are an important class of materials due to their unique physical and chemical properties. They are widely applied in the chemical and petrochemical industries as catalysts, adsorbents and ion exchangers [1,2]. The main applications of these materials come from the particular topology of their porous systems of molecular dimensions, prompting a strong interest in the synthesis of new zeolite topologies as well as in the control of the synthesis conditions in order to tailor the catalytic and adsorptive properties of the existing zeolite frameworks [3,4]. Organic molecules are commonly added to the synthesis gels in order to direct the crystallization pathway towards a particular zeolite framework, and therefore these organic molecules are usually referred to as structure directing agents (SDAs) [5–7]; however, a direct univocal relation between the SDA and the zeolite product is rarely found. SDA molecules are thought to organize the tetrahedral units around them generating the building blocks from which nucleation and growth of a particular zeolite structure takes place [8,9]. Traditionally, amines and quaternary ammonium cations have been the most widely used species as SDAs, although some ethers and tetraalkylphosphonium salts have also being employed [10,11]. Work carried out in our group has shown that changes in the chemical nature of the SDAs, like the addition of fluorine atoms, or the presence of co-structure directing agents, have a strong impact on the products of crystallization [12–14].

Research on the crystallization of zeolites by using chiral organic molecules or chiral complexes as SDAs has a particular interest in zeolite science, with the ultimate goal of transferring the chirality from the molecular component to the inorganic solid. Chiral zeolite frameworks would be of extreme importance because these solids could potentially perform enantioselective catalysis and separation processes [15]. For these enantioselective applications, the bulk material should be homochiral or enantioenriched to a significant degree, and hence the challenge is to control the crystallization process so that a significant enantiomeric excess of a potential chiral zeolite framework is achieved [16]. Although many chiral zeolite frameworks have been theoretically predicted [17], only few examples of chiral zeolite structures have been synthesized so far [18]. In this context, there are encouraging examples in the literature where the chiral organic template has transferred its chirality to the inorganic host. One of the most interesting chiral zeolite structures recently discovered is ITQ-37, which possesses an additional interest due to its extra large 30-ring windows, on the mesoporous range [19]. Although the molecule used as SDA for preparing this material was a meso-form, and hence achiral, it possessed four asymmetric

* Corresponding author. Tel.: +34 91 5854796; fax: +34 91 5854760.
E-mail address: rgs@icp.csic.es (R. García).

0920-5861/$ – see front matter © 2011 Elsevier B.V. All rights reserved.
doi:10.1016/j.cattod.2011.07.017

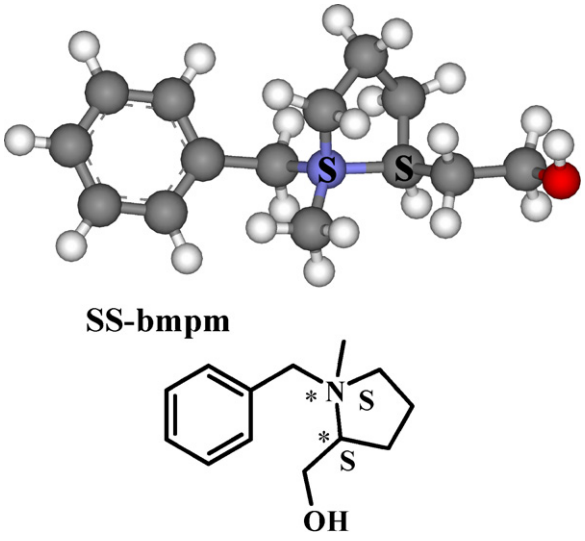

Fig. 1. Molecular structure of (1S,2S)-2-hydroxymethyl-1-benzyl-1-methylpyrrolidinium (SS-bmpm), highlighting the two asymmetric atoms.

centers on its molecular structure; however, to our knowledge, no catalytic results on asymmetric processes have been published so far with this new material. Davis and Lobo indicated that the use of a chiral template led to the synthesis of a beta zeolite (BEA) enriched in the chiral polymorph A [20]. This sample of zeolite beta was capable of performing enantioselective adsorption and catalysis, yielding a low although appreciable enantiomeric excess [20]. On the other hand, Morris and co-workers have successfully induced quirality in the ionothermal synthesis of a coordination polymer using a chiral ionic solvent [21]; besides, some chiral complexes are capable of imprinting chirality in the host materials [22]. In addition, theoretical calculations suggest that a particular chiral SDA, (S)-N-benzylpyrrolidine-2-methanol, arranges in a supramolecular helicoidal, and hence chiral, disposition when occluded within the AlPO-5 structure [23]. Therefore, the exploration of the use of chiral structure directing agents in zeolite synthesis as a route to chiral zeolite frameworks remains a mostly interesting topic.

We have been recently working on an alternative synthesis strategy, based on the use of co-structure directing agents (co-SDAs), i.e. a combination of two SDAs for the crystallization of a single zeolite structure: a bulky SDA and a smaller organic molecule or inorganic cation. The rationale behind this strategy is that the smaller co-SDA would facilitate the formation of small cages while the large SDA would direct the formation of larger channels, thus leading to complex structures with pore systems based on cages and channels [24]. Previous work showed that the use of the quaternary ammonium cation 1-benzyl-1-methylpyrrolidinium (bmp) as the bulky molecule enabled the crystallization of ferrierite or ferrierite-like materials depending on the organic molecule used as co-SDA [25,26], while the use of Na^+ as co-SDA together with bmp led to zeolites ZSM-12 and a mixture of ZSM-12 and beta [27]. All these results demonstrate the efficiency of this synthesis strategy for the crystallization of complex zeolite frameworks.

In the present work, we combine this synthesis strategy with the use of chiral SDAs in an attempt to lead the crystallization pathway towards complex zeolite structures, with the ultimate goal of obtaining chiral frameworks. We have recently studied the structure directing role of different diastereoisomers of the chiral cation 2-hydroxymethyl-1-benzyl-1-methylpyrrolidinium (bmpm, Fig. 1), which has a structure related to that of bmp and possesses two asymmetric centers in the molecule. We observed that the pure (1S,2S) diastereoisomer directs the crystallization of the 12-ring zeolite ZSM-12 in pure silica preparations [28]. We report here the results we have obtained using the SS-diastereoisomer of this chiral cation, (1S,2S)-2-hydroxymethyl-1-benzyl-1-methylpyrrolidinium (SS-bmpm), as the bulky SDA in aluminosilicate preparations in fluoride medium, either alone or in the presence of other co-structure directing agents.

2. Experimental

2.1. Synthesis of the organic SDA

The quaternary ammonium cation, (1S,2S)-2-hydroxymethyl-1-benzyl-1-methylpyrrolidinium iodide, was obtained through methylation of the commercially available amine (S)-1-benzyl-2-pyrrolidinemethanol (97 wt%, Aldrich), as described in Ref. [28]. The organic halide was anion-exchanged to give the corresponding hydroxide using an anionic resin (Amberlite IRN-78, exchange capacity: 4 mequiv./g, Supelco). The concentration of the resultant organic hydroxide (SS-bmpmOH) was determined by HCl (0.05 N, Panreac) titration using phenolphthaleine (Aldrich) as indicator.

2.2. Molecular sieve syntheses

Molecular sieves were prepared from gels of composition: 0.06 co-SDA:0.48 SS-bmpmOH:0.48 HF:$(x/2)$ Al_2O_3:$(1-x)$ SiO_2:4.3–4.7 H_2O, where Co-SDA stands for Na^+ (NaOH, Panreac, 97 wt%), quinuclidine (quinuclidinium hydrochloride, Aldrich 97 wt%) or TMA (TMAOH, Aldrich 25 wt%) and x was 0.06 for gels with Si/Al ~15 or 0.0324 for gels with Si/Al ~30. In a typical synthesis preparation, tetraethyl orthosilicate (TEOS, Merck 98 wt%) and aluminum isopropoxide (Fluka, 97 wt%) were added to a solution containing the two SDAs in a polypropylene flask. The solution was maintained with stirring until the ethanol coming up from the TEOS hydrolysis and the excess of water were evaporated. Subsequently, HF (48 wt%, Panreac) was added dropwise. The resulting thick gel was homogenized and introduced into 20-mL Teflon-lined stainless steel autoclaves which were heated statically at 135 °C or 150 °C under autogeneous pressure for selected periods of time (Table 1). The solid products were recovered by filtration, washed with water and ethanol and dried at room temperature overnight.

In order to remove the organic content, selected samples were heated in N_2 at 200 °C for 2 h, followed by a treatment with a flow of ozone/oxygen (60 mL/min, ca. 2 vol.% O_3) at 200 °C until complete removal of the organic content was achieved, as indicated by TGA. Ozone was produced using an ECO-5 ozone generator manufactured by SALVECO Proyectos, S. L.

Samples will be referred to with the name of the organic molecule employed as co-SDA, followed by the Si/Al ratio and by the conditions of the hydrothermal treatment (temperature and time). As an example, TMA-15-135/20d refers to the sample prepared with a Si/Al ratio of 15 in the gel, heated at 135 °C for 20 days using (1S,2S)-2-hydroxymethyl-1-benzyl-1-methylpyrrolidinium (SS-bmpm) and tetramethylammonium (TMA) as co-SDAs.

2.3. Characterisation

X-ray powder diffraction (XRD) patterns were collected with a Panalytical X'Pro diffractometer using Cu K_α radiation. Thermogravimetric analysis (TGA) was carried out using a Perkin-Elmer TGA7 instrument at a heating rate of 20 °C/min under air flow. Chemical analyses were obtained from a Perkin-Elmer 2400 CHN analyzer. Scanning electron microscopy and EDX analyses were carried out using a JEOL JSM 6400 Philips XL30 operating at 20 kV. Solid State Nuclear Magnetic Resonance MAS-NMR spectroscopy was performed on a Bruker AV 400 spectrometer, using a BL7 probe for ^{13}C. ^{1}H to ^{13}C cross polarization (CP) spectra were recorded using

Table 1
Gel compositions and products. The gel composition for the different samples was: 0.06 Co-SDA:0.48 SS-bmpmOH:0.48 HF:(x/2) Al_2O_3:(1 − x) SiO_2:4.3–4.7 H_2O, where co-SDA designates Na^+, quinuclidine (quin) or tetramethylammonium (TMA), and x was 0.06 for gels with Si/Al ∼ 15 or 0.0324 for gels with Si/Al ∼ 30. For preparations with SS-bmpm as the only SDA, the same molar composition was used but the molar ratio of SS-bmpmOH was 0.54 instead of 0.48.

Gel	Co-SDA	Si/Al gel	T (°C)	t (days)	Product
bmpm-15-135/25d	–	14.93	135	25	A[a]
bmpm-15-135/46d	–	14.93	135	46	A
bmpm-30-150/25d	–	30.2	150	25	A
bmpm-30-135/25d	–	30.2	135	25	A
bmpm-30-135/49d	–	30.2	135	49	A
Na-15-150/12d	Na^+	14.97	150	12	A
Na-15-150/25d	Na^+	14.97	150	25	LEV + A
Na-15-150/52d	Na^+	14.97	150	52	LEV + NON
Na-15-135/12d	Na^+	14.97	135	12	A
Na-15-135/52d	Na^+	14.97	135	52	LEV + A
quin-15-150/11d	quin	15.67	150	11	A
quin-15-150/21d	quin	15.67	150	21	A
quin-15-150/30d	quin	15.67	150	30	A
quin-15-135/11d	quin	15.67	135	11	A
quin-15-135/30d	quin	15.67	135	30	A
TMA-15-150/10d	TMA	15.66	150	10	MWW + FER
TMA-15-150/20d	TMA	15.66	150	20	MWW + FER
TMA-15-150/47d	TMA	15.66	150	47	NON (+FER)
TMA-15-135/20d	TMA	15.66	135	20	FER-type
TMA-15-135/47d	TMA	15.66	135	47	FER-type
TMA-30-150/10d	TMA	29.9	150	10	MWW (+MTN)
TMA-30-150/20d	TMA	29.9	150	20	MTN major
TMA-30-150/29d	TMA	29.9	150	29	MTN major
TMA-30-135/20d	TMA	29.9	135	20	A
TMA-30-135/29d	TMA	29.9	135	29	MWW + A

[a] A: amorphous.

π/2 rad pulses for proton of 4.5 μs and a recycle delay of 3 s; the samples were span at the magic angle (MAS) at a rate of 5–5.5 kHz.

2.4. Computational details

The computational methodology was based on a similar protocol that we have been recently using for studying structure directing effects in the crystallization of the FER structure [25,26]. The geometry of the fully condensed MWW structure (1 × 1 × 1 u.c.) has been kept fixed during all the calculations. Molecular structures and the interaction energies of the organic SDAs (TMA and SS-bmpm molecules) with the framework are described with the CVFF forcefield [23,25,26,29–31]. The atomic charges for the organic molecules were calculated by the charge-equilibration method [32], setting the total net molecular charge to +1. The positive charge of the organic SDA molecules was compensated by the framework by using a related version of the uniform charge background method [33], where the atomic charge for every silicon framework atom was reduced from 2.4 until charge neutrality. Framework oxygen charges were kept fixed to −1.2.

The most stable location for the SDA molecules was obtained by means of simulated annealing calculations. The interaction energy was then calculated by subtracting the energy of the molecules in vacuo to the total energy of the system.

3. Results and discussion

3.1. Synthesis and characterisation of zeolites

The use of SS-bmpm as the only SDA in the preparation of zeolites in fluoride medium from aluminosilicate gels resulted in the production of amorphous materials for the two Si/Al ratios (Si/Al = 15 and Si/Al = 30) and at the different crystallization conditions tested (Table 1), in contrast to the results observed for pure-silica gels that led to ZSM-12 materials [28]. Since the use of SS-bmpm as the only SDA was unsuccessful in these aluminosilicate preparations, a co-structure directing agent (co-SDA) was introduced in order to further explore the versatility of this synthetic approach and the ability of SS-bmpm to direct the crystallization of a zeolite. Three co-SDAs were employed in the preparations with SS-bmpm: two small organic molecules (TMA and quinuclidine) and an inorganic cation, Na^+. All the experiments were performed with a similar gel composition in order to compare the effect of a systematic change of the co-SDA. The synthesis gel compositions and the zeolite phases observed are listed in Table 1.

3.1.1. Synthesis using Na^+ as co-SDA

The presence of Na^+ cations as co-SDAs together with SS-bmpm led to the production of a zeolite crystalline phase, Levyne (LEV structure-type), after 25 days at 150 °C. Few diffractions corresponding to this phase were observed at this crystallization stage; an increase of the crystallization time to 52 days caused the co-crystallization of nonasil (NON structure-type). In contrast, a decrease of the temperature to 135 °C enabled the production

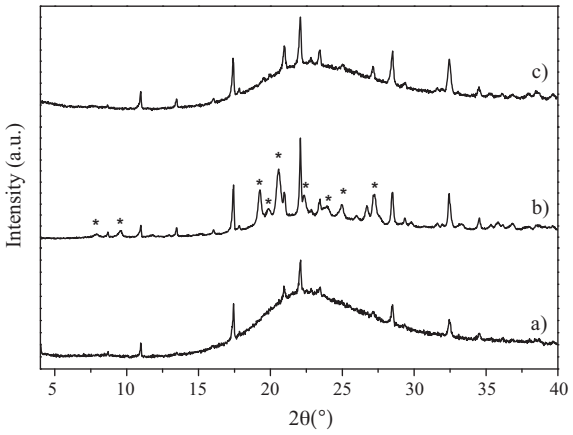

Fig. 2. X-ray diffraction pattern of samples (a) Na-15-150/25d (LEV and amorphous material), (b) Na-15-150/52d (LEV and NON) and (c) Na-15-135/52d (LEV and amorphous material) (* indicates diffractions of nonasil (NON)).

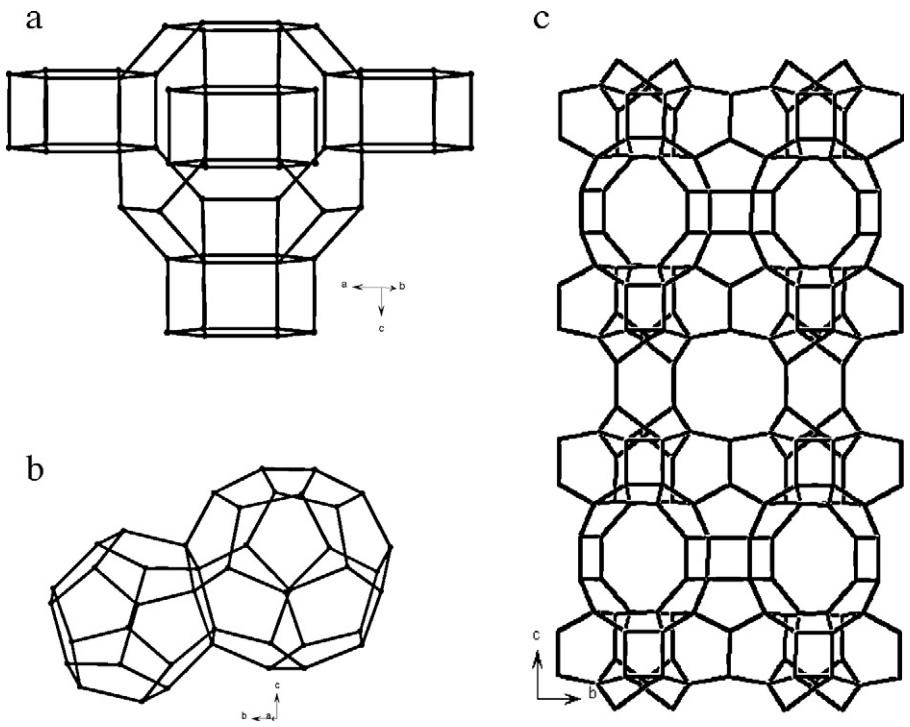

Fig. 3. Structure of relevant phases synthesized in this work: (a) Levyne (LEV), (b) Dodecasil 3C (MTN) and (c) MCM-22 (MWW).

of the LEV framework as a pure phase after 52 days (Na-15-135/52d), though the incoherent scattering phenomena observed in the region 15–35° 2θ (Fig. 2) indicated the presence of a large amount of an amorphous aluminosilicate phase.

Levyne is an Al-rich zeolite which possesses a two-dimensional channel system delimited by 8 membered-ring apertures. This zeolite belongs to the chabazite group: its framework can be built from layers of 6 membered-rings stacked along the [0 0 1] direction. The stacking sequence of these layers creates a heptadecahedral cage, the Levyne cage, outlined by nine 4-membered, five 6-membered and three 8-membered rings (Fig. 3a) [34]. The cage of this small pore material (with approximate dimensions of 7.3 Å × 6.3 Å × 6.3 Å) is not large enough as to host the chiral cation, with its longest dimension being around 11 Å. Indeed, CHN analysis of sample Na-15-135/52d (Table 2) gives a low C/N ratio (C/N ~ 7) compared to that of SS-bmpm (C/N ratio = 13), suggesting that the SS-bmpm molecule has decomposed under these hydrothermal conditions.

Fig. 4 shows the CP ^{13}C MAS NMR spectrum of sample Na-15-135/52d together with that of the pure SS-bmpm cation. Resonances between 50 and 70 ppm and those in the region between 15 and 30 ppm can be assigned to the prolinol ring; resonances due to the aromatic carbons (120–140 ppm) are also present in the spectrum. This suggests that although most of the SS-bmpm molecule might have decomposed, part of it might be retained either in the zeolite external surface or in the amorphous phase accompanying the sample; however, the low C/N ratio and the low intensity of the aromatic signals in the CP ^{13}C MAS NMR spectrum indicate that this is only a small fraction of the total organic content.

3.1.2. Synthesis using quinuclidine as co-SDA

Synthesis using quinuclidine as co-SDA did not result in the formation of any crystalline phase at the conditions employed. This result, as those shown above, suggests that SS-bmpm has a low structure-directing ability in aluminosilicate preparations, especially if compared with the related bmp cation that, under similar conditions, led to the crystallization of FER-type materials [26].

3.1.3. Synthesis using TMAOH as co-SDA

In contrast to previous results, the experiments performed in the presence of TMAOH as a co-SDA yielded crystalline products at relatively short crystallization times. At 150 °C, a mixture of zeolites ferrierite and MCM-22 – here MCM-22 designates a material of the MWW family [35] – crystallized after 10 days, although an increase of the synthesis time drove the system towards the formation of the clathrasil nonasil (NON), becoming the predominant phase at 47 days (Fig. 5). A decrease of 15 °C in the synthesis temperature

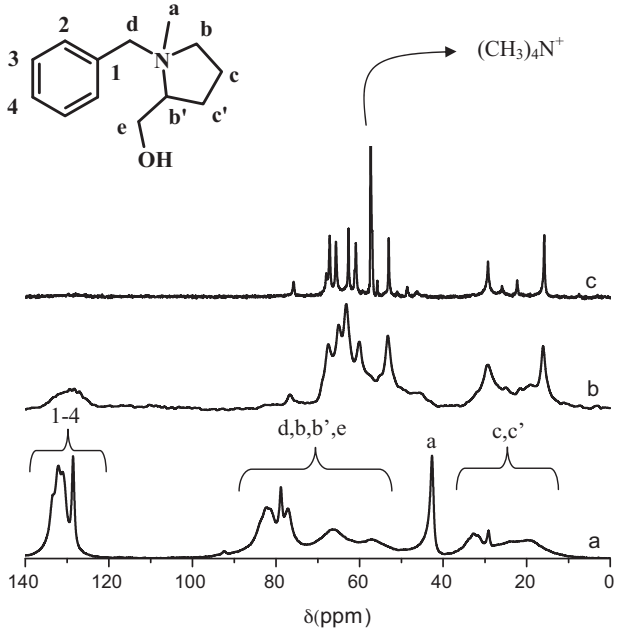

Fig. 4. CP ^{13}C MAS NMR of selected samples: (a) SS-bmpm cation; (b) sample Na-15-135/52d (LEV and amorphous material); (c) sample TMA-30-150/29d (mainly MTN).

Table 2
Chemical analysis (C, H, N and C/N molar ratio) and thermogravimetric analysis of representative samples. The C/N molar ratio of SS-bmpm and TMA are 13 and 4, respectively.

Sample	Zeolite	Chemical analyses				TGA (wt%)[a]
		C (wt%)	H (wt%)	N (wt%)	C/N (mol)	
TMA-30-135/29d	MWW	9.79	2.22	1.63	7.01	17.58
TMA-30-135/29d extracted	MWW	6.79	2.66	1.13	7.03	15.52
TMA-30-150/29d	MTN	3.43	1.56	0.92	4.37	5.25
Na-15-135/52d	LEV	8.46	2.12	1.42	6.95	17.05

[a] Weight loss in the temperature range $200 < T < 900\,^{\circ}C$.

(135 °C) results in a change of the phase selectivity, allowing the stabilization of a ferrierite related phase, whose details have been already reported [36].

Scanning electron microscopy images of sample TMA-15-150/20d (Fig. S1-a), a mixture of MCM-22 and FER, show the presence of hexagonal plates, the characteristic morphology of MCM-22 materials, and agglomerates of elongated crystals from the ferrierite phase. EDX analyses performed on the hexagonal crystals of MCM-22 indicated a Si/Al ratio of 18, slightly higher than that of the initial gel (Si/Al = 15.7). Ferrierite is an Al-rich zeolite, and hence, its formation should be disfavored at higher silicon contents. Therefore, in an attempt to obtain MCM-22 as a pure phase, we increased the Si/Al ratio of the initial gel to 30. Results showed that a mixture of MCM-22 and the clathrasil Dodecasil 3C (MTN) crystallized after 10 days at 150 °C, although the latter becomes the predominant phase at longer crystallization times (Table 1; Fig. 6).

SEM images of the sample obtained after 30 days (Fig. S1-b) show the crystals of MTN as big spherical aggregates, with a Si/Al ratio of 32.7, close to the nominal value of the gel.

Dodecasil 3C (MTN) is a small-pore zeolite, a clathrasil material, with a structure comprising two types of cages, a smaller pentagonal dodecahedron and a larger hexadecahedron, which are fused through 5-ring windows [37] (Fig. 3b). There are 16 [5^{12}] and 8 [$5^{12}6^4$] cages per MTN unit cell. Although their structures are very different, the basic building unit for MWW and MTN is the 12 membered-ring double cups [37], suggesting a structural relationship between the two phases that co-crystallize. TMA has been reported as SDA for Dodecasil 3C [38], suggesting that the presence of this cation might favor the crystallization of this phase. This is further supported by CHN analysis (Table 2, sample TMA-30-150/29d) that reveals a C/N of ~4 (the same as isolated TMA) and by

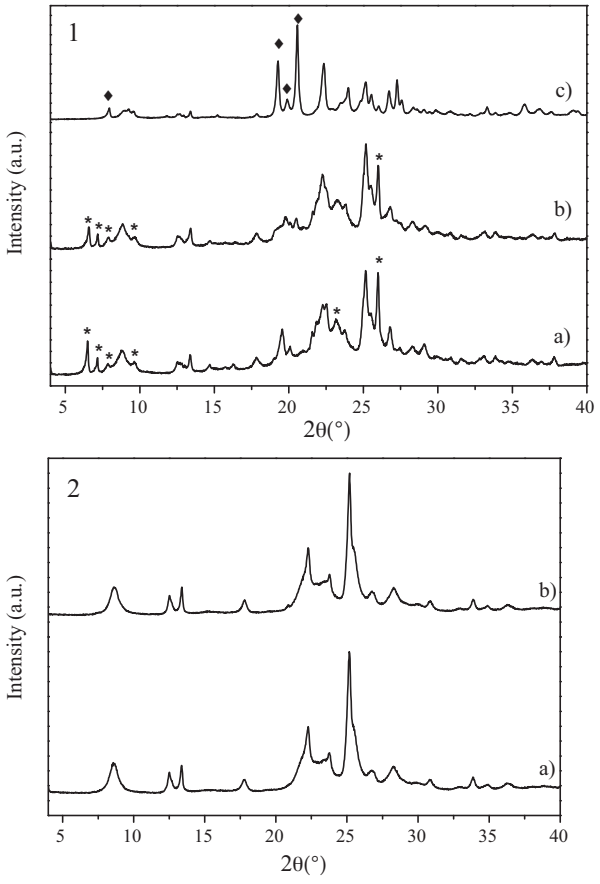

Fig. 5. X-ray diffraction patterns of samples synthesized in the presence of TMAOH as co-SDA for Si/Al = 15. (1) Experiments at 150 °C: (a) TMA-15-150/10d (mixture of MWW and FER), (b) TMA-15-150/20d (mixture of MWW and FER), (c) TMA-15-150/47d (mixture of NON and FER). (2) Synthesis at 135 °C: (a) TMA-15-135/20d (FER); (b) TMA-15-135/47d (FER) (* indicates diffractions of MWW; ♦ indicates diffraction of NON).

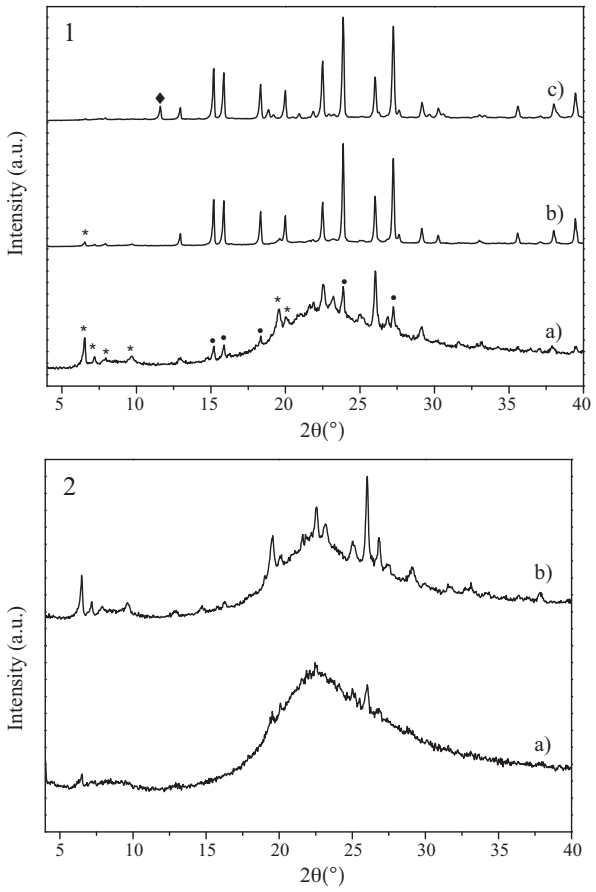

Fig. 6. X-ray diffraction patterns of samples synthesized in the presence of TMAOH as co-SDA for Si/Al = 30. (1) Experiments at 150 °C: (a) TMA-30-150/10d (mixture of MWW and MTN), (b) TMA-30-150/20d (mixture of MTN and MWW), and (c) TMA-30-150/29d (mainly MTN). (2) Synthesis at 135 °C: (a) TMA-30-135/20d (MWW and amorphous phase), (b) TMA-30-135/29d (MWW and amorphous phase) (* indicates diffraction peaks of MCM-22 (MWW); ● indicates diffraction peaks of MTN; ♦ unidentified product).

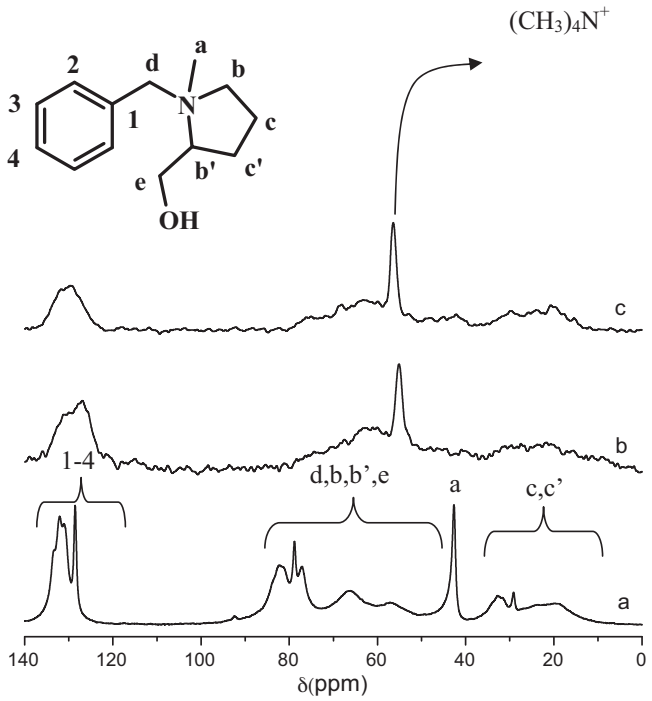

Fig. 7. CP ^{13}C MAS NMR of: (a) SS-bmpm cation; (b) as-prepared TMA-30-135/29d sample; (c) sample TMA-30-135/29d-extracted (sample TMA-30-135/29d after the acid treatment).

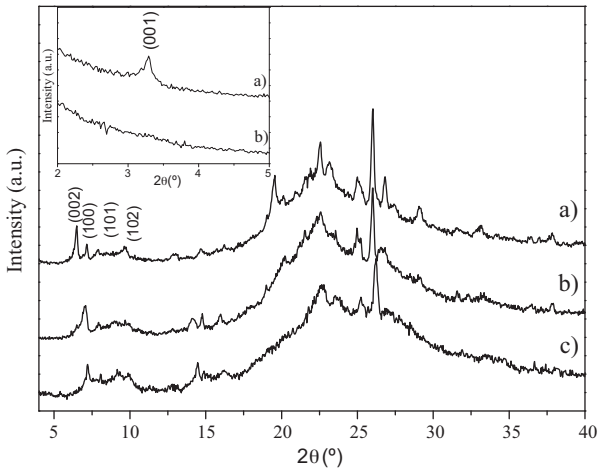

Fig. 8. XRD pattern of (a) as made TMA-30-135/29d; (b) TMA-30-135/29d-extracted and (c) TMA-30-135/29d-calcined. The inset figure shows the low angle XRD pattern of samples (a) and (b).

CP ^{13}C MAS NMR (Fig. 4). The spectrum of the sample does not show resonances arising from the aromatic groups (in the 120–160 ppm region), thus evidencing the cleavage of the SS-bmpm molecule that does not resist this long hydrothermal treatment at high temperature (150 °C). However, signals arising from the prolinol ring are observed together with an additional signal at 57.4 ppm, which is characteristic of the chemical shift of the TMA cation occluded in zeolite cages [39]. This spectrum suggests, therefore, that TMA and a fragment of the prolinol ring remained occluded within the structure. The complete combustion of the organic content occluded in the clathrasil is difficult, as shown in the TGA analysis (Fig. S2 of Supporting Information). A small weight loss (~5 wt%) can be observed between 200 and 900 °C, which has not finished at 900 °C due to the difficulty of the organic to escape out of the [$5^{12}6^4$] cages through the 6 membered-rings. This incomplete combustion is probably the reason for the low C/N ratio (~4) obtained for this sample by CHN analysis, despite the presence of the prolinol fragment as evidenced by CP ^{13}C NMR.

A decrease of the crystallization temperature to 135 °C had a noteworthy effect, leading to the crystallization of MCM-22(P) as a pure phase for the Si/Al content of 30. A rather slow crystallization rate was observed and even after 29 days, the XRD pattern of the sample (TMA-30-135/29d) shows the presence of a considerable amount of amorphous material. The XRD pattern of the as made solid is consistent with the one reported for MCM-22(P). The diffraction peaks can be indexed by comparison with those reported for this material: a low diffraction peak at $2\theta \sim 3.30^\circ$ can be assigned to the (0 0 1) diffraction, and the diffraction peaks at 2θ of 6.53°, 7.21°, 7.96° and 9.78° correspond to (0 0 2), (1 0 0), (1 0 1) and (1 0 2) diffractions, respectively, resulting in approximate unit cell parameters of $a = b = 14.17$ Å and $c = 27.17$ Å, in agreement with those found for related materials [35]. SEM images of this sample (Fig. S1-c) show crystals of MCM-22(P) as hexagonal plates with a Si/Al ratio of 24 (as determined by EDX).

MCM-22 (MWW structure-type) is a very interesting zeolite, which usually crystallizes as a layered precursor (MCM-22(P)) that forms a three-dimensionally connected framework upon calcination. There is a whole family of materials with a topology related to that of MWW, such as MCM-56, MCM-49, MCM-22(P), ITQ-30 or EMM-10 [35,40–45]. The difference between these materials comes from the packing arrangement of the layers [35]. MCM-22(P) usually crystallizes with layers composed of one unit cell along the *c*-direction (orthogonal to the layers) stacked in vertical alignment, which appear to be connected through hydrogen bonding between surface silanols [35]. MCM-56 material is made up by disordered/misaligned monolayers of the MWW structure [43]; the recently discovered EMM-10 material is composed by layers stacked without vertical alignment [44]; MCM-49 is instead considered to be the three dimensionally connected material [45].

CP ^{13}C MAS NMR of sample TMA-30-135/29d evidenced the presence of the two SDAs in the sample (Fig. 7). The chemical shift of the methyl carbon atoms of TMA in MCM-22 (sample TMA-30-135/29) appeared between −56 and −55 ppm, similar to that of the free TMA ions ($\delta \sim -55$ ppm) [39], suggesting that the organic cation is not very tightly confined. The CHN analysis gives a C/N ratio of 7, between that of the two organic molecules used as SDAs (C/N = 13 for SS-bmpm and 4 for TMA), consistent with the presence of both cations in the sample, as evidenced by CP ^{13}C MAS NMR. The organic content of the material, as determined from the weight loss observed in TGA between 200 and 900 °C, is 17.58 wt%.

It has been shown that a mild acid treatment of the lamellar precursor MCM-22(P) can partially remove the organic material located between the MWW sheets, what disturbs their parallel arrangement and cause the formation of a structure analogous to MCM-56 [46,47]. Following this result, we subjected the TMA-30-135/29d sample to a mild extraction treatment, stirring the sample overnight in a mixture of diluted HCl (0.1 M) and ethanol at room temperature, in an attempt to induce an approximation of the layers. The X-ray diffraction pattern of the product obtained (TMA-30-135/29d-extracted) significantly changed compared to that of the as prepared material (Fig. 8). This was mostly reflected by the disappearance of the low angle diffraction at $2\theta \sim 3.30^\circ$, yielding a material with a lower unit cell along the *c* direction (the *c* parameter decreased from 27.17 to 25.06 Å), thus indicating an approach of the layers probably caused by a partial removal of organic material located between them. Indeed, even though the material undergoes a considerable loss of crystallinity upon calcination (Fig. 8), the diffraction pattern of the extracted product is closer to that of

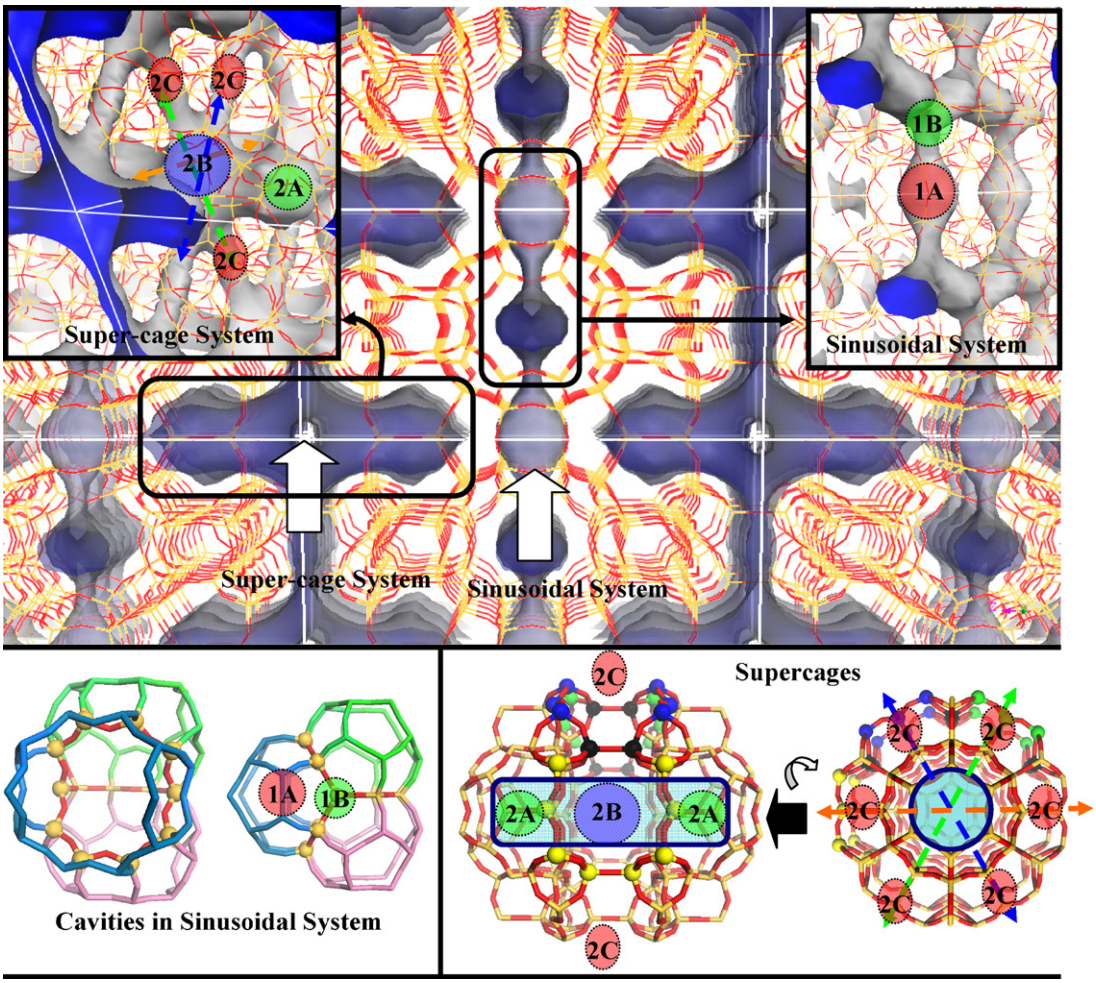

Fig. 9. *Top*: Topological description of MWW structure, showing the sinusoidal and the super-cage systems (free volume is shown in blue). *Bottom*: Detail of the topological features of the two channel systems, and label of the different types of positions where the SDAs can be accommodated, as described in the text. (For interpretation of the references to color in this figure legend, the reader is referred to the web version of the article.)

the calcined solid. TGA (Table 2) shows a ~2% reduction of the total organic content after the extraction treatment. The presence of SS-bmpm and TMA in the sample after the extraction was confirmed by CP ^{13}C MAS NMR (Fig. 7).

3.2. Molecular modeling

In general, synthesis of MCM-22 materials with a mixture of structure directing agents has been performed using a combination of a bulky organic molecule [48,49], as trimethyladamantammonium, and a smaller amine, as hexamethyleneimine. In those preparations, the bulky cation was too big to fit in the sinusoidal channel system and was expected to reside in the super-cages of the structure. In contrast, the structure directing agents used in this work, TMA, a small cation, and SS-bmpm, larger but with a high flexibility, could in principle fit in both systems, in the sinusoidal channels or in the super-cages. A computational study was then carried out in order to provide insights into the possible location of these SDAs within the material. Due to the complexity of this type of materials and the lack of knowledge about the disposition of the layers in our precursor material because of the presence of the amorphous phase, the computational study considered the fully condensed material, i.e. the structure of the calcined MWW. We are aware that this represents only an approximate model of our system, but we think it might help to understand the crystallization of this material in the presence of the two different molecules.

The void volume of the MWW structure is conformed by two independent channel systems, one formed by sinusoidal 10-MR channels that will be referred to as sinusoidal system, and another one formed by super-cages and straight 10-MR channels, hereafter designated super-cage system (Fig. 9). These two channel systems are not interconnected, and therefore the occlusion of the SDA molecules can be studied independently on each system.

3.2.1. Occlusion of SDA molecules within the sinusoidal system

We now consider the occlusion of the SDA molecules, TMA and SS-bmpm, within the sinusoidal system. In principle, there are two different sites to locate the SDA molecules in this system, in the middle of the cavity (position 1A in Fig. 9), or in the intersection between the three adjacent cavities (position 1B). The interaction energies of one TMA molecule occluded in the two positions were −71.2 and −37.6 kcal/mol per TMA molecule in positions 1A and 1B, respectively, evidencing a much higher stability of TMA located in position 1A, and hence that TMA will only reside in this position, i.e. within the cavities. The final location of the molecules within each site is shown in Fig. 10 (top), where we can appreciate the structural relationship between the shape of the cavity (see Fig. 9 top-right, inset) and that of TMA, hence explaining the high stability of TMA in this site. If we now load one TMA molecule per cavity – which corresponds to 3 TMA in the sinusoidal system per MWW unit cell – the interaction energy becomes −174.7 kcal/mol per MWW unit cell (see Fig. 10, bottom-left). Incorporation of a fourth TMA molecule

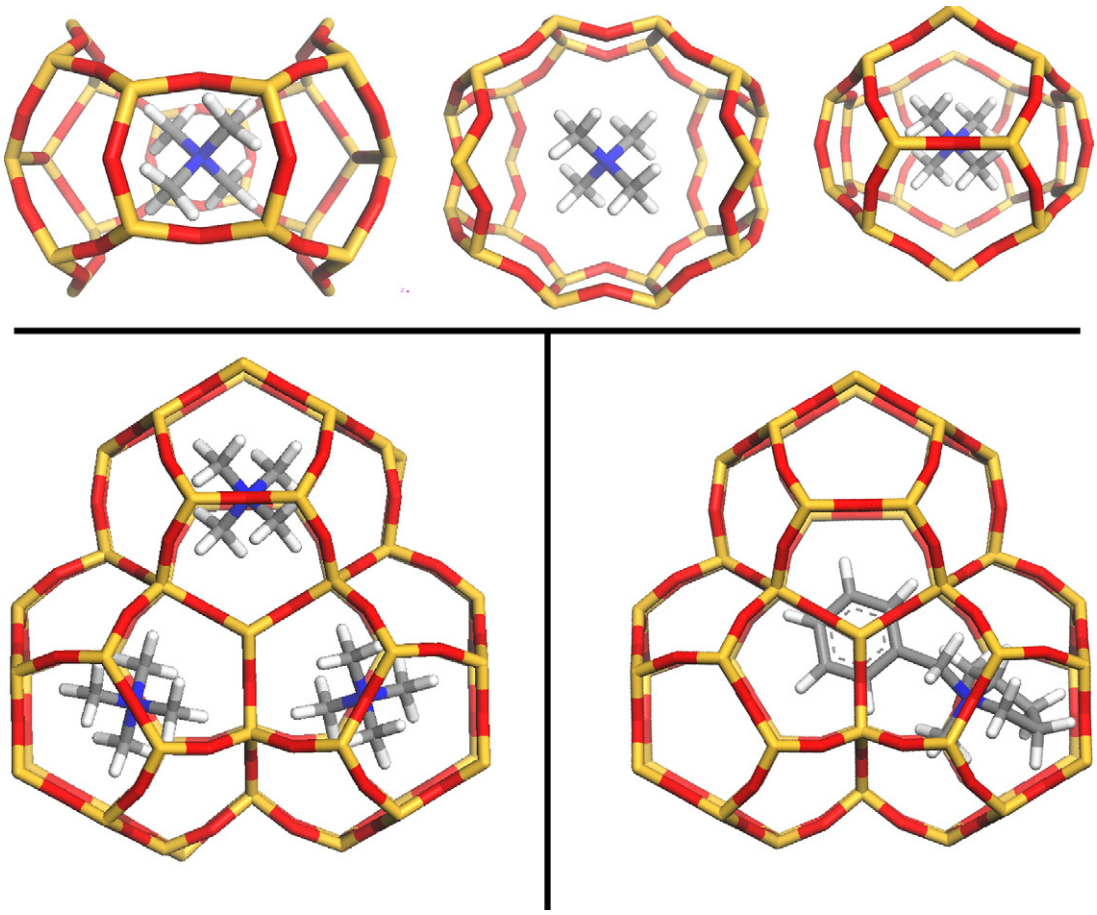

Fig. 10. *Top*: Three views of the location of TMA within the cavities of the sinusoidal system. *Bottom-left*: Arrangement of TMA molecules within adjacent cavities of the sinusoidal system. *Bottom-right*: SS-bmpm located within the cavities of the sinusoidal system.

within this system, located in position 1B, in addition to the other 3 TMA located in position 1A, resulted in a very unstable system, with an interaction energy of −77.8 kcal/mol per unit cell, evidencing that there is only space to accommodate 3 TMA molecules per unit cell, i.e. one TMA per cavity, in the sinusoidal system.

We now tried to incorporate the larger molecule, SS-bmpm, within this channel system; in principle, one SS-bmpm molecule per MWW unit cell was loaded. The final location of SS-bmpm is shown in Fig. 10 (bottom-right): the pyrrolidine ring of SS-bmpm sites in the middle of one of the cavities (position 1A, see Fig. 9), while the benzyl ring sites in the intersection of three adjacent cavities, in position 1B. The interaction energy of SS-bmpm located in this position is −72.5 kcal/mol per unit cell. We then tried to load a second SS-bmpm molecule in a single MWW unit cell (2 SS-bmpm per unit cell), but all attempts resulted in the cleavage of the molecule upon geometry optimisation. A lower loading of 1.5 SS-bmpm per unit cell was also tried (3 SDA molecules in 2 MWW unit cells), and the interaction energy was now −59.6 kcal/mol, lower than that of 1 molecule per unit cell (−72.5 kcal/mol), demonstrating that the maximum SS-bmpm content within the sinusoidal system is one molecule per unit cell.

The interaction energy developed between the SDAs and the MWW structure (with SDAs only in the sinusoidal system) is much higher if it is loaded with TMA (−174.7 kcal/mol per MWW unit cell, with 3 TMA per unit cell) than when it is loaded with SS-bmpm (−72.5 kcal/mol per MWW unit cell, with only 1 molecule per unit cell). This large energy difference, together with the much higher stability of SS-bmpm molecules within the super-cages, as will be seen below, suggest that, during the synthesis, only TMA will be incorporated within the cavities of the sinusoidal system.

3.2.2. *Occlusion of SDA molecules within the super-cage system*

We now consider the occlusion of the SDA molecules within the super-cage system. In this case, there are three different sites to locate the SDA molecules (Fig. 9), in the middle of the large super-cage (position 2B, blue circle), in the lateral side-pocket cavities of the super-cage (position 2A, green circles), or within the 10-MR channels that connect adjacent super-cages (position 2C, red circles).

We first studied the incorporation of TMA molecules within this system. TMA located in position 2B results in an interaction energy of −116.9 kcal/mol, while in position 2A the interaction energy is −103.4 kcal/mol. Position 2C is the most unfavorable for TMA, with an interaction energy of −50.1 kcal/mol. Therefore, it becomes clear that TMA, if occluded during the synthesis in the super-cage system, will be located in the super-cages, either in the center (position 2B) or in the lateral side-pockets (position 2A).

We then studied the incorporation of SS-bmpm. The larger size of this SDA molecule involves that it can only be incorporated in positions 2B or 2A. The interaction energies found for the two positions were −139.4 and −145.5 kcal/mol for positions 2B and 2A, respectively. Site 2C is instead too small to host this large SDA molecule (the interaction energy was −13.0 kcal/mol, evidencing that in this case, the 10-MR channels are too narrow to accommodate the large co-SDA). Fig. 11 shows the final location of the SS-bmpm molecule sited in positions 2B and 2A.

Next a second SS-bmpm molecule was loaded. All attempts to load a second molecule when the first one was located in position 2B, in the center of the large cavity, resulted in the molecules being cleaved upon geometry optimisation, evidencing that only one SS-bmpm molecule can be accommodated in this position. However,

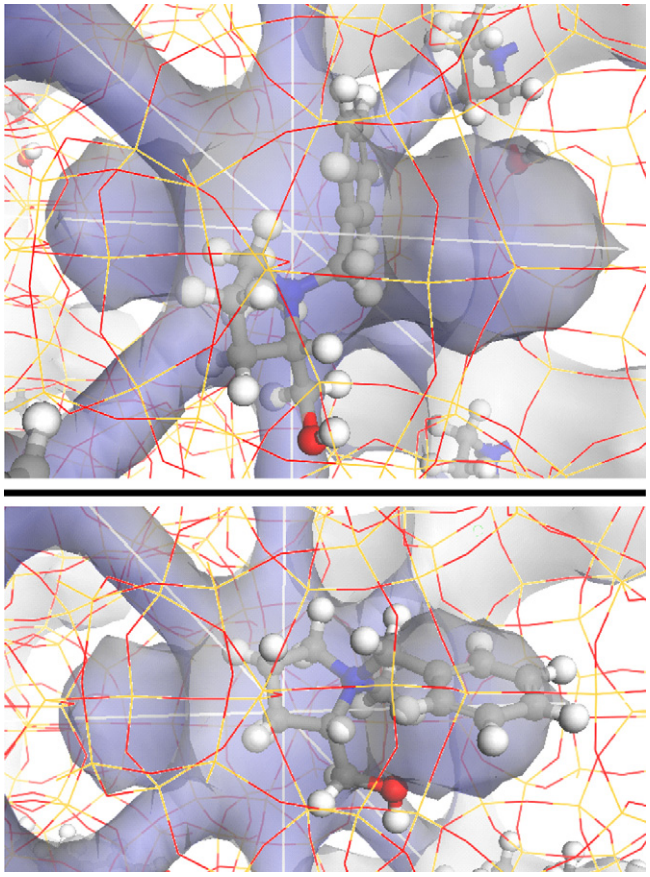

Fig. 11. Location of SS-bmpm in the super-cages, in position 2B (top), and in position 2A (bottom); for easiness of visualisation, the free volume is shown in violet. (For interpretation of the references to color in this figure legend, the reader is referred to the web version of the article.)

if the molecule is located in position 2A, this arrangement allows for the incorporation of a second SS-bmpm molecule, in the other side pocket of the super-cage. Two different relative orientations of the two SS-bmpm molecules are possible, with the two aromatic rings facing each other ('phfac'), or with the pyrrolidine rings in the center of the super-cage ('phopp'). The interaction energies of the two arrangements were −281.7 and −283.7 kcal/mol per MWW unit cell for 'phfac' and 'phopp' orientations, respectively, showing a similar stability for both intermolecular orientations. Fig. 12 (left) shows the location of the 2 SS-bmpm molecules in the two orientations, where we can observe an efficient space-filling of the cavities, and therefore no additional TMA molecules can be located within the super-cage.

A different case is observed if the first SS-bmpm molecule is sited in position 2B (Fig. 11-top). As previously mentioned, this molecular arrangement does not allow for the incorporation of a second SS-bmpm molecule; however, observation of the void space suggests that two TMA molecules could be accommodated in addition to the SS-bmpm sited in position 2B, one TMA on each of the side-pockets (positions 2A). This configuration (Fig. 12-right) resulted in an interaction energy of −360.2 kcal/mol per MWW unit cell.

It is not straightforward to compare the stability of the two configurations due to their different relative organic compositions – the different amount of molecules occluded – and the different stability of the two types of molecules in the synthesis gel. In this case, the energy difference between the two types of configurations is not as large as in the sinusoidal system, and therefore we could not discriminate with confidence between the two, suggesting that any of them could in principle occur, at least from a thermodynamic point of view.

In summary, the computational study indicates that the sinusoidal system will be only filled with TMA molecules, loading 3 TMA per unit cell in the cavities. However, two possibilities exist for the guest composition of the super-cage system, either 2 SS-bmpm molecules or 2 TMA and 1 SS-bmpm molecules per super-cage, i.e. per MWW unit cell. The computational study did not allow for establishing a preferential occupation of the super-cages by any of the two types of guest compositions. Besides, we could not compare the theoretical C/N ratio and N content of the two different compositions with those observed experimentally by CHN analysis due to the large amount of amorphous material present in the sample.

3.2.3. *Effect of the interlayer separation on the location of SDA molecules*

Following our study on the FER structure [26,50], we wanted to have an idea about the effect of the separation of the mono-layers that is known to occur in the as-prepared sample, as evidenced by decrease of the '*c*' parameter upon extraction, on the location and interaction energies of the SDA molecules. As mentioned throughout the paper, the large amount of amorphous material in our

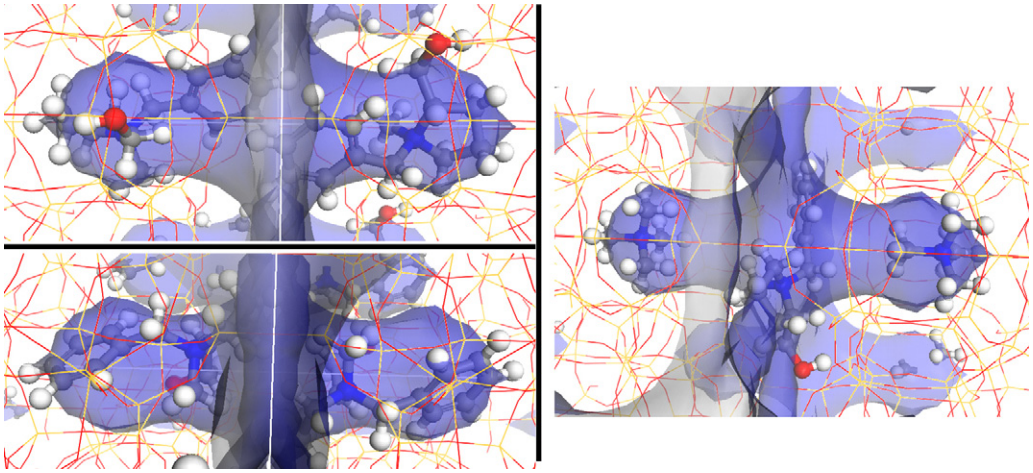

Fig. 12. Location of 2 SS-bmpm molecules within the super-cages in positions 2A, with benzyl rings facing each other (left-top, 'phfac') or in opposite sides (left-bottom, 'phopp'), and location of 2 TMA (in position 2A) and one SS-bmpm (in position 2B); for easiness of visualisation, the free volume is shown in violet. (For interpretation of the references to color in this figure legend, the reader is referred to the web version of the article.)

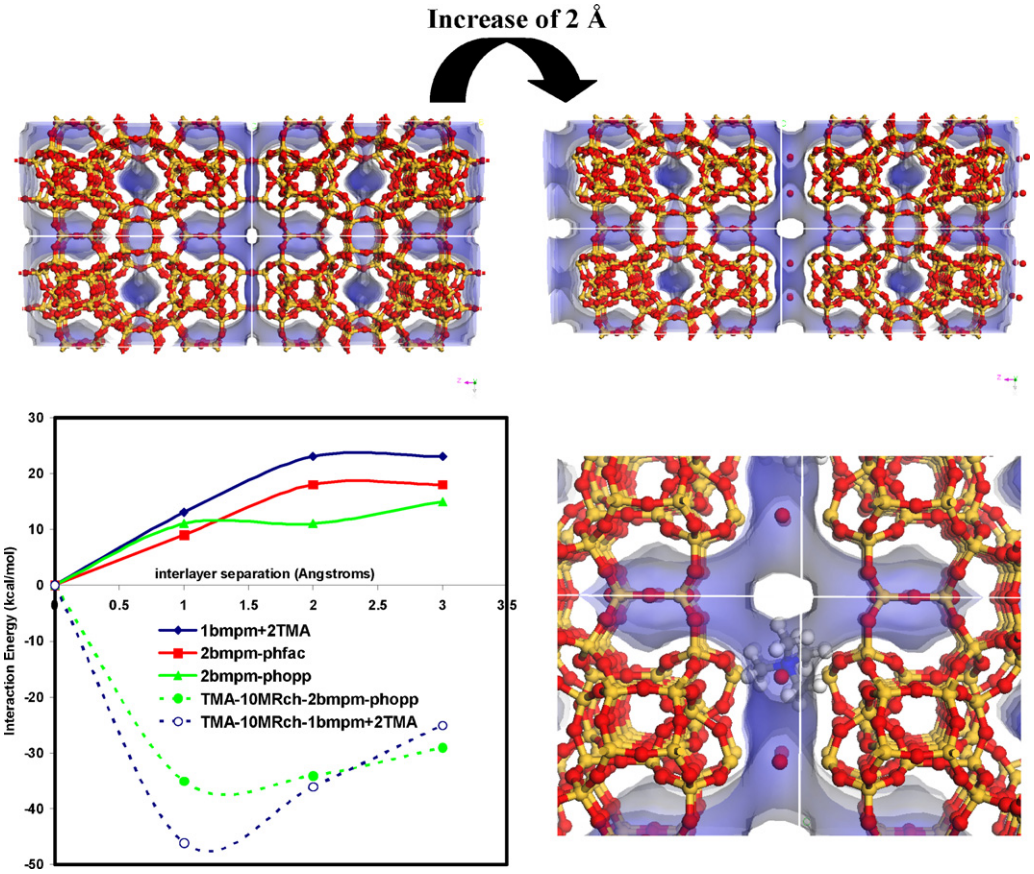

Fig. 13. Effect of the layer separation on the void space of MWW (*top*: left: fully condensed MWW; right: layers separated by 2 Å) and on the interaction energies of the SDAs (bottom-left: solid lines indicate the supercages loaded with 1 SS-bmpm and 2 TMA (blue) or 2 SS-bmpm (red and green); dashed lines are the systems where an additional TMA is loaded in the straight 10-MR channels of the super-cage system). Bottom-right: location of TMA in the 10-MR channels (molecules in the super-cage are not shown for the sake of clarity). (For interpretation of the references to color in this figure legend, the reader is referred to the web version of the article.)

sample did not allow to get a reliable conclusion about the stacking of the layers in the as-prepared material: it could take place in an ordered or disordered fashion. From a computational point of view, we could only simulate the simpler case, a separation of the layers giving place to an ordered precursor, which is known to occur in other MWW materials [35]; indeed, the use of simplifications is common when computationally studying MWW related materials [51]. In any case, we still think that this model is useful to gain insights on the effect of a layer separation on the void space of the structure that could help to understand the crystallization of this type of precursors. Besides, four different diffractions assigned to (0 0 2), (1 0 0), (1 0 1) and (1 0 2) can be appreciated in the XRD pattern of our as-prepared sample, suggesting at least a partial ordering of the MWW layers. On the other hand, the computational methodology used did not allow to study the actual linking between the layers, we just kept them as in the MWW structure, but separated by 1 Å steps, with the central O equidistant to the two layers.

Results are shown in Fig. 13. The main effect of the layer separation on the MWW void space is reflected in the straight 10-MR channels of the super-cage system (this system is the only one affected by the layer separation), which are notably enlarged (Fig. 13-top). We calculated the interaction energies of the molecules located in the super-cage, in the same compositions and orientations as before, i.e. 1 SS-bmpm + 2TMA (blue) or 2 SS-bmpm in 'phfac' (red) or in 'phopp' (green) orientations (Fig. 13-bottom-left). Results indicate a decrease of the interaction of the molecules with the framework in all cases upon the layer separation, probably due to the reduction of the confinement effect caused by the larger distance between the layers, what would suggest a lower stability of the SDA molecules in the precursor. We observed that no additional SDA molecules can be occluded within the super-cage after the layer separation. However, as previously mentioned, the layer separation involves a notable increase of the 10-MR channel dimensions. We showed in Section 3.2.2 the instability of TMA located in these channels (position 2C) in the fully condensed material. An increase of the interlayer distance brings a large stabilisation of this TMA position, as evidenced by the increase of the interaction with the interlayer distance in systems where we loaded an additional TMA in such positions (Fig. 13-bottom-left, dashed lines). These results suggest that, at least in an ordered layered precursor, a new position becomes available in the 10-MR channels when the layers are separated by 2 Å (Fig. 13-bottom-right). Indeed, the presence of these TMA molecules in the interlayer space could explain the decrease of the organic content (2%) that occurs upon the extraction treatment that leads to the approximation of the layers.

4. Conclusions

In this work, we have explored the structure directing effect of the chiral cation (S,S)-2-hydroxymethyl-1-benzyl-1-methylpyrrolidinium (SS-bmpm) in aluminosilicate preparations in the presence of co-structure directing agents. In the presence of sodium cations, zeolite Levyne was obtained as a consequence of the partial cleavage of the cation, while preparations with quinuclidine yielded amorphous solids. The presence of TMA as a co-SDA yielded crystalline phases, a ferrierite related material and a mate-

rial from the MWW family, where the SS-bmpm and the TMA cations remained incorporated intact within the samples.

A computational study based on molecular mechanics calculations provided some insights about the possible filling of the void space in the complex MWW structure by the co-SDA molecules. The computational results indicate that TMA molecules fill the cavities of the sinusoidal system, while the bulkier SS-bmpm molecules would locate exclusively in the super-cages of the structure. Our model also suggests that the MWW precursors with an ordered disposition of the layers can accommodate TMA molecules within the 10-MR channels of the super-cage system, but these positions disappear when the layers approach and are partially condensed.

Acknowledgments

We are thankful for the financial support of the Spanish Ministry of Science and Innovation MICINN, Project MAT-2009-13569. L. Gómez-Hortigüela acknowledges Ministerio de Ciencia y Tecnología for a Juan de la Cierva contract. Accelrys is acknowledged for providing the software and Centro Técnico de Informática for running the calculations.

Appendix A. Supplementary data

Supplementary data associated with this article can be found, in the online version, at doi:10.1016/j.cattod.2011.07.017.

References

[1] M.E. Davies, Nature 417 (2002) 813.
[2] A. Corma, Chem. Rev. 95 (1995) 559.
[3] S.T. Wilson, Stud. Surf. Sci. Catal. 170A (2007) 3.
[4] A. Corma, M.E. Davies, ChemPhysChem 5 (2004) 304.
[5] R.F. Lobo, S.I. Zones, M.E. Davis, J. Inclusion Phenom. Mol. Recognit. Chem. 21 (1995) 47.
[6] R.F. Lobo, M.E. Davis, Chem. Mater. 4 (1992) 756.
[7] H. Gies, B. Marler, Zeolites 12 (1992) 42.
[8] C.S. Cundy, P.A. Cox, Chem. Rev. 103 (2003) 663.
[9] A.V. Goretsky, L.W. Beck, S.I. Zones, M.E. Davis, Micropor. Mesopor. Mater. 28 (1999) 387.
[10] S.L. Burkett, M.E. Davis, Micropor. Mater. 1 (1993) 265.
[11] A. Corma, M.J. Diaz-Cabanas, J.L. Jorda, F. Rey, G. Sastre, K.G. Strohmaier, J. Am. Chem. Soc. 130 (2008) 16482.
[12] L. Gomez-Hortigüela, J. Perez-Pariente, T. Blasco, Micropor. Mesopor. Mater. 78 (2005) 189.
[13] M. Arranz, J. Perez-Pariente, T. Blasco, Micropor. Mesopor. Mater. 89 (2006) 235.
[14] R. Garcia, M. Arranz, T. Blasco, J. Perez-Pariente, Micropor. Mesopor. Mater. 114 (2008) 312.
[15] M.E. Davis, Top. Catal. 25 (2003) 3.
[16] R.E. Morris, X. Bu, Nat. Chem. 2 (2010) 353.
[17] Y.J. Yu, Z. Wang, J. Zhang, M. Guo, R. Xu, Chem. Mater. 17 (2005) 4399.
[18] J. Yu, R. Xu, J. Mater. Chem. 18 (2008) 4021.
[19] J. Sun, C. Bonneau, A. Cantín, A. Corma, M. Díaz-Cabañas, M. Moliner, D. Zhang, M. Li, X. Zhou, Nature 458 (2009) 1154.
[20] M.E. Davis, R.F. Lobo, Chem. Mater. 4 (1992) 756.
[21] Z. Lin, A.M.Z. Slawin, R.E. Morris, J. Am. Chem. Soc. 129 (2007) 4880.
[22] Y. Wang, J. Yu, Y. Li, Z. Shi, R. Xu, Chem. Eur. J. 9 (2003) 5048.
[23] L. Gómez-Hortigüela, F. Córa, C.R.A. Catlow, J. Pérez-Pariente, Phys. Chem. Chem. Phys. 8 (2006) 486.
[24] J. Pérez-Pariente, R. García, A.B. Pinar, L. Gómez-Hortigüela, E. Sastre, C. Márquez-Alvarez, Stud. Surf. Sci. Catal. 174A (2008) 135.
[25] A.B. Pinar, L. Gomez-Hortiguela, J. Perez-Pariente, Chem. Mater. 19 (2007) 5617.
[26] R. García, L. Gómez-Hortigüela, I. Díaz, E. Sastre, J. Pérez-Pariente, Chem. Mater. 20 (2008) 1099.
[27] R. García, I. Díaz, J. Pérez-Pariente, Micropor. Mesopor. Mater. 118 (2009) 273.
[28] R. García, L. Gómez-Hortigüela, F. Sánchez, J. Pérez-Pariente, Chem. Mater. 22 (2010) 2276.
[29] P. Dauger-Osguthorpe, V.A. Roberts, D.J. Osguthorpe, J. Wolff, M. Genest, A.T. Hagler, Proteins: Struct. Funct. Genet. 4 (1988) 21.
[30] E.C. Moloy, R.T. Cygan, F. Bonhomme, D.M. Teter, A. Navrotsky, Chem. Mater. 16 (2004) 2121.
[31] J.J. Williams, C.W. Smith, K.E. Evans, Z.A.D. Lethbridge, R.I. Walton, Chem. Mater. 19 (2007) 2423.
[32] A.K. Rappe, W.A. Goddard III, J. Phys. Chem. 95 (1995) 3358.
[33] A. De Vita, M.J. Gillan, J.S. Lin, M.C. Payne, I. Stich, J.L. Clarke, Phys. Rev. B 46 (1992) 12964.
[34] S. Merlino, E. Galli, A. Alberti, TMPM Tschermaks Mineral. Petrogr. Mitt. 22 (1975) 117;
P. Caullet, L. Delmotte, A.C. Faust, J.L. Guth, Zeolites 15 (1995) 139.
[35] W.J. Roth, D.L. Dorset, Micropor. Mesopor. Mater. 142 (2011) 32.
[36] R. García, L. Gómez-Hortigüela, F. Sánchez, J. Pérez-Pariente, Micropor. Mesopor. Mater., doi:10.1016/j.micromeso.2011.04.041, in press.
[37] H. van Koningsveld, H. Gies, Z. Kristallogr. 219 (2004) 637.
[38] J.L. Schlenker, F.G. Dwyer, E.E. Jenkins, W.J. Rohrbaugh, G.T. Kokotailo, Nature 294 (1981) 340.
[39] S. Hayashi, K. Suzuki, K.J. Hayamizu, J. Chem. Soc., Faraday Trans. 85 (1989) 2973.
[40] A. Corma, M.J. Díaz-Cabañas, M. Moliner, C. Martínez, J. Catal. 241 (2006) 312.
[41] R. Millini, G. Perego, W.O. Parker Jr., G. Bellussi, L. Carluccio, Micropor. Mater. 4 (1995) 221.
[42] W.J. Roth, J. Cejka, Catal. Sci. Technol. 1 (2011) 43.
[43] G. Juttu, R.F. Lobo, Micropor. Mesopor. Mater. 40 (2000) 9.
[44] W.J. Roth, D.L. Dorset, G.J. Kennedy, Micropor. Mesopor. Mater. 142 (2011) 168.
[45] S.L. Lawton, A.S. Fung, G.J. Kennedy, L.B. Alemany, C.D. Chang, G.H. Hatzikos, D.N. Lissy, M.K. Rubin, H.C. Timken, S. Steuernagel, D.E. Woessner, J. Phys. Chem. 100 (1996) 3788.
[46] Y. Wang, Y. Liu, L. Wang, H. Wu, X. Li, M. He, P. Wu, J. Phys. Chem. C 113 (2009) 18753.
[47] L. Wang, Y. Wang, Y. Liu, L. Chen, S. Cheng, G. Gao, M. He, P. Wu, Micropor. Mesopor. Mater. 113 (2008) 435.
[48] M.A. Camblor, A. Corma, M.J. Díaz-Cabañas, C. Baerlocher, J. Phys. Chem. B 102 (1998) 44.
[49] S.I. Zones, S.-J. Hwang, M.E. Davis, Chem. Eur. J. 7 (2001) 1991.
[50] R. García, L. Gómez-Hortigüela, T. Blasco, J. Pérez-Pariente, Micropor. Mesopor. Mater. 132 (2010) 375.
[51] G. Sastre, C.R.A. Catlow, A. Chica, A. Corma, J. Phys. Chem.B 104 (2000) 416.